Journal of
Materials Sciences and Applications

Research Article Open Access

Fabrication of Layered Crystal Structure $Li_{1-x}Ni_{1-x-y}Mn_xCo_yO_2$ ($0.1 \le x+y \le 0.5$) with Homogeneous Arrangement of Ni^{3+}, Mn^{4+}, and Co^{3+}, as well as its Battery Performances

Dong-Heon Lee[1,2], Huan-Hee Yoo[1,3] and Kyoo-Seung Han[1,*]

[1]Department of Chemical Engineering and Applied Chemistry, Chungnam National University, 99 Daehak-ro, Yuseong-gu, Daejeon, Republic of Korea

[2]Daejeon Jungbu Police Station, 112 Jungang-ro, Jung-gu, Daejeon, Republic of Korea

[3]Cathode Material Development Team 3, LG Chem, 88 Munji-ro, Yuseong-gu, Daejeon, Republic of Korea

[*]**Corresponding Author:** Kyoo-Seung Han, Department of Chemical Engineering and Applied Chemistry, Chungnam National University, 99 Daehak-ro, Yuseong-gu, Daejeon, Republic of Korea, Tel: +82-42-821-5897, E-mail: kshan@cnu.ac.kr

Received Date: August 21, 2023 **Accepted Date:** September 21, 2023 **Published Date:** September 23, 2023

Citation: Dong-Heon Lee, Huan-Hee Yoo, Kyoo-Seung Han (2023) Fabrication of Layered Crystal Structure $Li_{1-x}Ni_{1-x-y}Mn_xCo_yO_2$ ($0.1 \le x+y \le 0.5$) with Homogeneous Arrangement of Ni^{3+}, Mn^{4+}, and Co^{3+}, as well as its Battery Performances. J Mater sci Appl 7: 1-15

Abstract

Intrinsic disadvantages of $LiNi_{1-x-y}Mn_xCo_yO_2$ such as an inappropriate but stable oxidation state of Ni^{2+}, as well as a heterogeneous arrangement of Ni, Mn, and Co within $LiNi_{1-x-y}Mn_xCo_yO_2$ are overcome by the solubility control according to coprecipitation temperature for homogeneous arrangement of Ni, Mn, and Co, as well as the selective oxidation control from Ni^{2+} to Ni^{3+} without changing the states of Co^{3+} and Mn^{4+}. The novel $Li_{1-x}Ni_{1-x-y}Mn_xCo_yO_2$ ($0.1 \le x + y \le 0.5$) prepared through the selective oxidation has a single-phase layered crystal structure with a space group R3m. The battery performance of the $Li_{1-x}Ni_{1-x-y}Mn_xCo_yO_2$ with homogeneous arrangement of Ni^{3+}, Mn^{4+}, and Co^{3+} shows a maximum available capacity of 262 mAh/g and a capacity retention rate of 99.7% in 40 charging and discharging cycles.

Keywords: Lithium Secondary Battery; Cathode Materials; Lithium Transition Metal Oxide**;** Layered Crystal Structure; Selective Oxidation

Introduction

Humans pursue goals endlessly, and efforts to achieve them are expressed as energy conversion in any form. The representative ability of mankind is that mankind knows how to use tools, and mankind is making efforts to use tools as the most effective way to achieve its goals. Naturally, energy conversion is also necessary for the operation of the tool. Energy is neither created nor dissipated, just convertible. Efficient tool operation is realized through the highest efficiency energy conversion, and the energy associated with the highest conversion efficiency is electrical energy. Therefore, since the most efficient tool is electronic devices, electronic devices are indispensable to mankind for efficient and convenient life. It is generally overlooked or misunderstood that an electronic device without a battery, whether direct or indirect, may not exist. A battery is a device that converts various types of energy into electrical energy using chemical reactions, radiation, temperature differences, light activity, power, etc.

Because it is easy to design and manufacture lithium secondary batteries to best suit properties such as energy density, capacity, power, safety, life cycle, price, etc. depending on the unique demands of various electronic devices, they can be applied as a power source for a wide variety of electronic devices that require a wide range of energy density and power density.

Chemical formulas of commercially representative cathode materials, such as a layered crystal structure lithium transition metal oxide, a spinel-type crystal structure lithium transition metal oxide, and an olivine-type crystal structure lithium transition metal phosphate, can be abbreviated as $LiMO_2$ (M = Ni, Mn, Co, etc.), LiM'_2O_4 (M' = Mn, Ni, Co, etc.), $LiM''PO_4$ (M" = Fe, Mn, Ni, Co, etc.), respectively. Here, all of the M, M', and M" are 3*d* transition metals. This is because 3*d* transition metals have higher electrode potential than 4*d* and 5*d* transition metals, are relatively lightweight and small in size, which are advantageous in terms of battery capacity per unit weight and per unit volume [1].

Layered crystal structure $LiNi_{1-x-y}Mn_xCo_yO_2$ ($0.1 \leq x + y \leq 0.5$) may exhibit a theoretical and also available capacity of up to 280 mAh/g as well as sustainable battery performances [1,2]. To obtain such $LiNi_{1-x-y}Mn_xCo_yO_2$, two significant challenges need to be addressed.

The first challenge is to ensure homogeneity in the arrangement of Ni, Mn, and Co within $LiNi_{1-x-y}Mn_xCo_yO_2$. A liquid reaction producing method can be easily and homogeneously mixed Ni, Mn, and Co in atomic units. As a solid reaction producing method, Ni, Mn, and Co cannot be homogeneously mixed in atomic units, and as a vapor phase reaction producing method, Ni, Mn, and Co can be homogeneously mixed in atomic units, but it is impossible to produce a powder-type cathode active material, and a film-type cathode active material can be produced. During charging and discharging of a lithium secondary battery made of $LiNi_{1-x-y}Mn_xCo_yO_2$ as a cathode active material, Ni, Mn, and Co are oxidized and reduced in different sequences. When the arrangement of Ni, Mn, and Co within $LiNi_{1-x-y}Mn_xCo_yO_2$ is heterogeneous, it can decrease the available capacity and shorten the overall battery lifespan. To overcome this issue, many efforts have been attempted, such as developments of particles achieving a concentration-gradient Ni, Mn, and Co as well as a hybridized shape of Ni-rich core and Mn-rich shell [3,4]. Regrettably, a cathode active material with a concentration-gradient Ni, Mn, and Co has not registered a noticeable market share.

The second challenge is the selective oxidation number control of nickel. Only when the average oxidation number of Ni, Mn, and Co of $LiNi_{1-x-y}Mn_xCo_yO_2$ is +3 or slightly higher than +3, $LiNi_{1-x-y}Mn_xCo_yO_2$ may have a layered crystal structure and maintain charge neutrality. Cobalt ion prefers the electron configuration of Co^{3+}, while nickel and manganese ion prefers the electron configuration of Ni^{2+} and Mn^{4+} to Ni^{3+} and Mn^{3+} [1,5]. In the case of $LiNi_{1-x-y}Mn_xCo_yO_2$ with high nickel ratio, single-phase layered crystal structure $LiNi_{1xy}Mn_xCo_yO_2$ containing Ni^{2+} cannot be generated. Thus, three-dimensional crystal structure $Li_{1-z}Ni_{1-x-y+z}Mn_xCo_yO_2$ in which Li^+ and Ni^{2+} are mixed in a non-stoichiometric ratio in each other, not in their own position, and/or impurities such as $Li_{1+z}Ni_{1-x-y-z}Mn_xCo_yO_2$ are inevitably mixed [1,6,7]. Therefore, only selective oxidation from Ni^{2+} to Ni^{3+} are required without altering the oxidation number of cobalt and manganese ions. Although it is known that one of the fundamental disadvantages of $LiNi_{1-x-}$

$_yMn_xCo_yO_2$ is an inappropriate but stable oxidation state of Ni^{2+}, many indirect efforts have been made to solve this disadvantage, but unfortunately, there is no direct effort to solve this disadvantage [8-12]. It's important to note that the layered crystal structure $LiNi_{1-x-y}Mn_xCo_yO_2$ is composed of a stacked combination of $Ni_{1-x-y}Mn_xCo_yO_2$ layers and LiO_2 layers.

In this study, the solubility control depending temperature of coprecipitation conditions for homogeneous arrangement of Ni, Mn, and Co and the process conditions for only selective oxidation from Ni^{2+} to Ni^{3+} without altering the oxidation number of cobalt and manganese ions were established at the same time.

Experimental

A fabrication of a layered crystal structure $Li_{1-x}Ni_{1-x-y}Mn_xCo_yO_2$ ($0.1 \le x + y \le 0.5$) with homogeneous arrangement of Ni^{3+}, Mn^{4+}, and Co^{3+} may be summarized into three ways.

Homogeneous Arrangement of Ni, Mn, and Co in the $Ni_{1-x-y}Mn_xCo_y$ Coprecipitation Granules Through a Rapid Hydroxide Coprecipitation Method in 58^{0}C Aqueous Solution of Nickel Sulfate, Manganese Sulfate, and Cobalt Sulfate

The solubility of various Li salts and transition metal salts was evaluated according to temperature. For the production of $Li_{1-x}Ni_{1-x-y}Mn_xCo_yO_2$ ($0.1 \le x + y \le 0.5$) with homogeneous arrangement of Ni, Mn, and Co using a liquid reaction method, the evaluated solubilities were relatively compared to determine Ni salt, Mn salt, and Co salt having the same solubility at a specific temperature. These results are shown in Figure 1 and 2.

As shown in Figure 2, nickel sulfate, manganese sulfate, cobalt sulfate, and iron sulfate have the same solubility in 58^{0}C water. However, lithium sulfate and aluminium sulfate have a slightly lower solubility than nickel sulfate, manganese sulfate, cobalt sulfate, and iron sulfate in 58^{0}C water. The small difference in solubility between lithium sulfate and nickel/manganese/cobalt sulfates in 58^{0}C water indicates that aqueous ionization solution solgel synthesis method cannot be applied to the preparation method of single-phase layered crystal structure $Li_{1-x}Ni_{1-x-y}Mn_xCo_yO_2$. The same solubility of nickel sulfate, manganese sulfate, and cobalt sulfate in 58^{0}C water represents that a precursor for producing $Li_{1-x}Ni_{1-x-y}Mn_xCo_yO_2$ with homogeneous arrangement of Ni, Mn, and Co can be produced through a rapid hydroxide coprecipitation method in 58^{0}C aqueous solution of nickel sulfate, manganese sulfate, and cobalt sulfate.

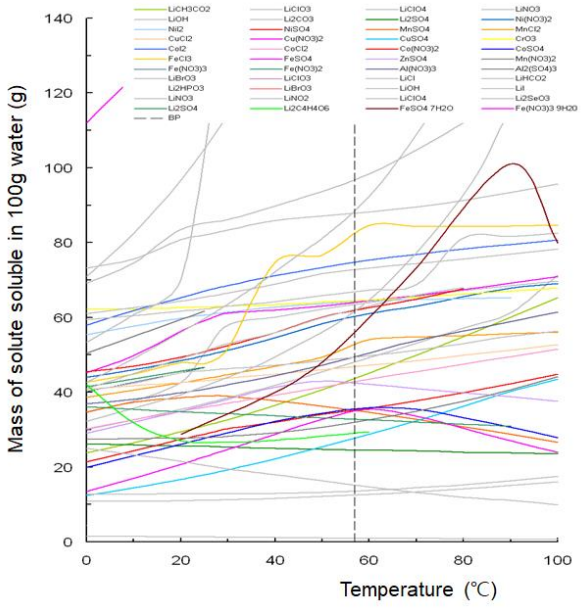

Figure 1: Solubility of various Li salts and transition metal salts in 100g of water according to temperature

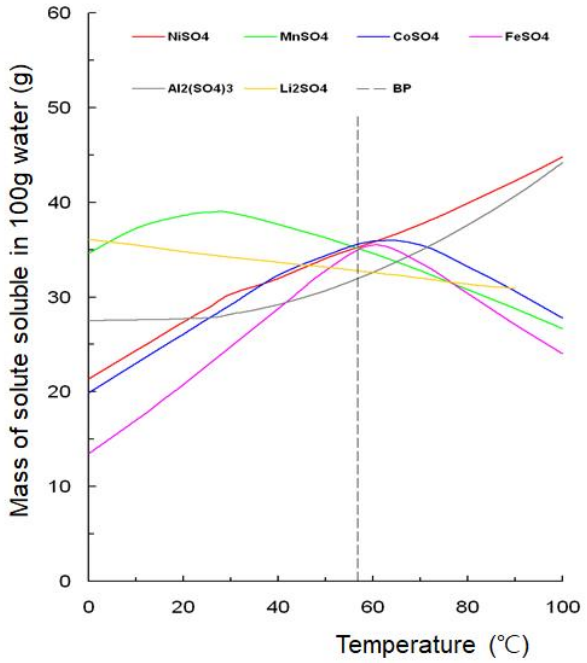

Figure 2: Solubility of lithium sulfate, nickel sulfate, manganese sulfate, cobalt sulfate, iron sulfate and aluminium sulfate in 100g of 58^0C water

A mixed aqueous solution of potassium hydroxide (KOH), ammonium hydroxide (NH_4OH), and sodium hydroxide (NaOH) was selected as alkaline aqueous solutions for rapid hydroxide coprecipitation. Mixing molar ratio of potassium hydroxide (KOH), ammonium hydroxide (NH_4OH), and sodium hydroxide (NaOH) depends on the molar ratio of Ni, Mn, and Co in $Li_{1-x}Ni_{1-x-y}Mn_xCo_yO_2$, as well as a fabrication amount. Here, it should be considered that the following three risk factors must be overcome. Since sodium ions have a smaller ionic radius than potassium ions, they may remain even after several filtrations and washings in the process of recovering secondary coprecipitation granules (result of collection, occlusion, and adsorption of primary coprecipitation particles). Because the remained sodium ions in secondary coprecipitation granules evidently remain in $Li_{1-x}Ni_{1-x-y}Mn_xCo_yO_2$ as cathode active material, they adversely affect lithium ion battery performances. Therefore, it is recommended to minimize the content of sodium hydroxide. Potassium hydroxide aqueous solution has the disadvantage of being highly toxic. In addition, ammonium hydroxide helps to uniformize particle size, collect primary particles, and spheroidize granules, but when its amount is excessive, it has a negative effect.

Selective Oxidation of Ni^{2+} up to Ni^{3+} without Changing the States of Co^{3+} and Mn^{4+} in Secondary Coprecipitation Granules

According to the characteristics of nickel ion and cobalt ion in the layered crystal structure $LiNi_{1-x-y}Mn_xCo_yO_2$, both nickel ion and cobalt ion are located in the octahedral sites surrounded by six oxygen ions, have a low spin electron configuration, as well as an electronpairing energy (P) and an energy difference between t_{2g} and e_g orbital energy levels noted as 10Dq or Δ_{oct} is in a 6Dq < P < 10Dq relationship for nickel ion, and in a P < 6Dq relationship for cobalt ion. The crystal field stabilization energy is -18Dq + P for Co^{2+}, 24Dq + 2P for Co^{3+}, and -20Dq + 2P for Co^{4+}. Therefore, a cobalt ion prefers the most stable electron configuration of Co^{3+}. By the way, a nickel ion has the crystal field stabilization energy of 12Dq for Ni^{2+}, 18Dq + P for Ni^{3+}, and -24Dq + 2P for Ni^{4+}, so it prefers the most stable electron configuration of Ni^{2+} [1]. A manganese ion prefers the most stable electron configuration of Mn^{4+}.

In order that the average oxidation number of Ni, Mn, and Co of $LiNi_{1-x-y}Mn_xCo_yO_2$ ($0.1 \leq x + y \leq 0.5$) is +3 or slightly higher than +3, the oxidation number of Ni in the $LiNi_{1-x-y}Mn_xCo_yO_2$ should be +3.

Oxidants capable of increasing the oxidation state of transition metal ions such as Ni, Mn, and Co include potassium permanganate ($KMnO_4$), sodium perborate ($NaBO_3$), sodium perchlorate ($NaClO_4$), sodium chlorate ($NaClO_3$), sodium chlorite ($NaClO_2$), and sodium hypochlorite (NaClO). However, none of these oxidants selectively oxidized Ni^{2+} to Ni^{3+} without changing the states of Co^{3+} and Mn^{4+}. These oxidants oxidized Co^{3+} to Co^{4+} and/or Ni^{2+} even further to Ni^{4+}. Therefore, in order to control their oxidation power, various oxidizing agent-reducing agent hybrid composites were prepared by adding agent lower than their oxidation power with a different amount and then evaluated. As a result, a mixed aqueous solution of NaClO and hydrogen peroxide (H_2O_2) could selectively oxidize Ni^{2+} to Ni^{3+} without changing the states of Co^{3+} and Mn^{4+} of the secondary coprecipitation granules. The optimal mixing ratio and each concentration of the NaClO and H_2O_2 aqueous solutions vary depending on the composition mole ratio of Ni, Mn, and Co, as well as the amount of the secondary coprecipitation granules. However, if the concentration of the mixed aqueous solution of NaClO and H_2O_2 is higher than 0.05M, dissolution of the secondary coprecipitation granules may occur.

Fabrication of $Li_{1-x}Ni_{1-x-y}Mn_xCo_yO_2$ with Homogeneous Arrangement of Ni^{3+}, Mn^{4+}, and Co^{3+}

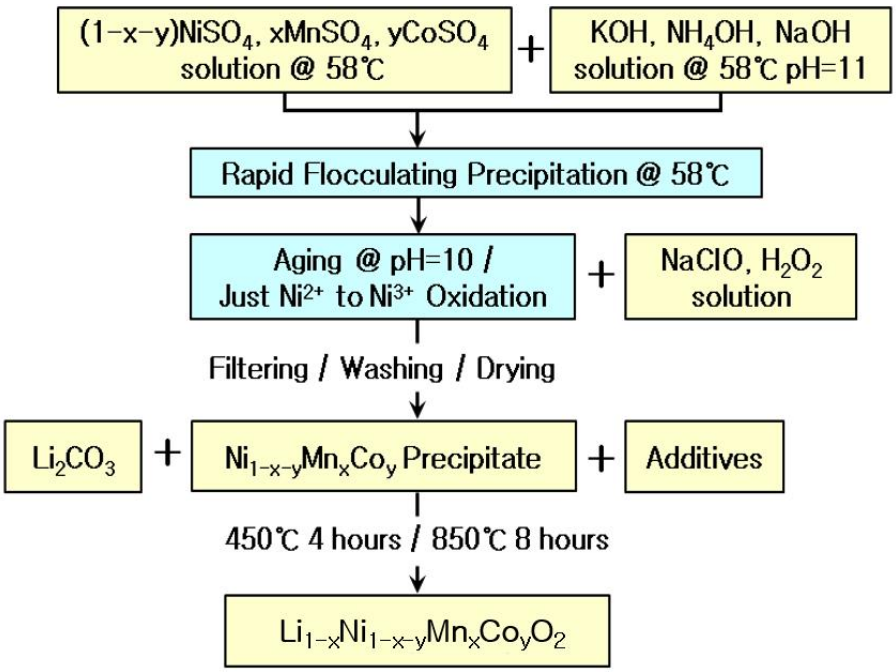

Figure 3: Fabrication process of $Li_{1-x}Ni_{1-x-y}Mn_xCo_yO_2$ ($0.1 \le x + y \le 0.5$) with homogeneous arrangement of Ni^{3+}, Mn^{4+}, and Co^{3+}

Figure 3 shows the fabrication process diagram of $Li_{1-x}Ni_{1-x-y}Mn_xCo_yO_2$ ($0.1 \le x + y \le 0.5$) with homogeneous arrangement of Ni^{3+}, Mn^{4+}, and Co^{3+}. During the mixing of the secondary coprecipitation granules ($Ni_{1-x-y}Mn_xCo_y$ coprecipitate) and Li_2CO_3, sucrose is added as an additive to prevent the agglomeration of the $Li_{1-x}Ni_{1-x-y}Mn_xCo_yO_2$ powders. The mixed molar ratio of Li_2CO_3, secondary coprecipitation granules, and sucrose is 0.525 : 1 : 0.1.

The prepared $Li_{1-x}Ni_{1-x-y}Mn_xCo_yO_2$ ($0.1 \le x + y \le 0.5$) is characterized by means of Xray diffraction (XRD) spectroscopy, inductively coupled plasma-mass spectroscopy (ICP-MS), X-ray absorption near edge structure (XANES) spectroscopy, extended X-ray absorption fine structure (EXAFS) spectroscopy, and Li magic angle spin nuclear magnetic resonance (Li MAS NMR) spectroscopy.

Electrochemical lithium intercalation and deintercalation experiments of the prepared $Li_{1-x}Ni_{1-x-y}Mn_xCo_yO_2$ ($0.1 \le x + y \le 0.5$) were realized by charge and discharge of coin type lithium secondary batteries using a mixture of the products (94% in weight) with SuperP/VGCF (3% in weight) and polyvinylidene fluoride (PVdF, 3% in weight) as cathode, lithium foil as anode and a 1 M $LiPF_6$ solution in

ethylene carbonate (EC) and ethyl methyl carbonate (EMC) (1 : 2, volumetric ratio) as electrolyte.

Results and Discussion

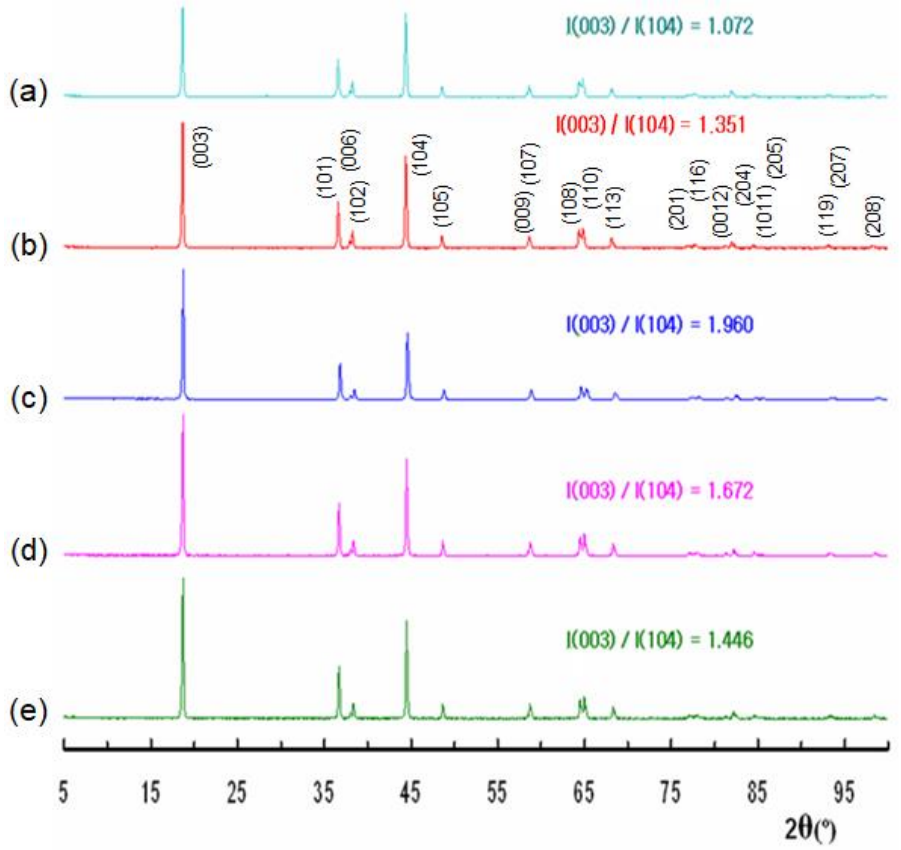

Figure 4: XRD patterns of (a) commercialized $LiNi_{0.8}Mn_{0.1}Co_{0.1}O_2$, (b)(e) $Li_{0.9}Ni_{0.8}Mn_{0.1}Co_{0.1}O_2$ manufactured according to the change in the mixing ratio and concentration of NaClO and H_2O_2 aqueous solution

Figure 4 illustrates the X-ray diffraction (XRD) pattern of commercialized $LiNi_{0.8}Mn_{0.1}Co_{0.1}O_2$ and $Li_{0.9}Ni_{0.8}Mn_{0.1}Co_{0.1}O_2$ manufactured according to the change in the mixing ratio and concentration of NaClO and H_2O_2 aqueous solution under the conditions for keeping the states of Ni^{3+}, Mn^{4+}, and Co^{3+}.

The intensity ratio of the (003)/(104) diffraction peaks, symbolized as I(003)/I(104), for commercialized $LiNi_{0.8}Mn_{0.1}Co_{0.1}O_2$ is lower than the cation mixing recognition criterion of 1.2, but I(003)/I(104) for all four $Li_{0.9}Ni_{0.8}Mn_{0.1}Co_{0.1}O_2$ is higher than 1.2. The results of I(003)/I(104) and [I(006)+I(102)]/I(101) Bragg peak intensity analysis, as well as peak splits in the (006)/(102) and (108)/(110) doublets, and show that all four $Li_{0.9}Ni_{0.8}Mn_{0.1}Co_{0.1}O_2$ do not contain a representative impurity with a space group $P3_112$ structure as well as the cation mixing phenomenon do not occur in the all four $Li_{0.9}Ni_{0.8}Mn_{0.1}Co_{0.1}O_2$ [13-15]. Thus, the XRD analysis reveals that all four $Li_{0.9}Ni_{0.8}Mn_{0.1}Co_{0.1}O_2$ have a single-phase layered crystal structure with a space group R-3m despite changes in the mixing ratio and concentration. These results indirectly show the successful preparation of $Li_{0.9}Ni_{0.8}Mn_{0.1}Co_{0.1}O_2$ with Ni^{3+}, Mn^{4+}, and Co^{3+}.

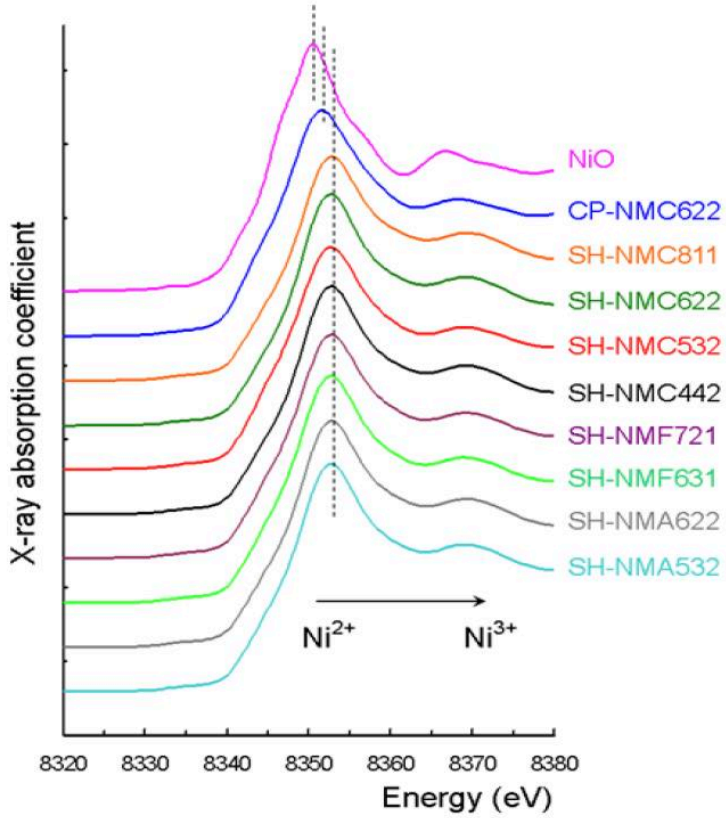

Figure 5: Ni X-ray absorption near edge structure (XANES) spectroscopic results of NiO, commercialized $LiNi_{1-x-y}Mn_xCo_yO_2$ manufactured by the general coprecipitation-heat treatment method (CP-NMC), and $Li_{1-x}Ni_{1-x-y}Mn_xCo_yO_2$ prepared by this study (SH-NMC)

Figure 5 illustrates the Ni X-ray absorption near edge structure (XANES) spectroscopic results of NiO, commercialized $LiNi_{1-x-y}Mn_xCo_yO_2$ manufactured by the general coprecipitation-heat treatment method (CP-NMC), and $Li_{1-x}Ni_{1-x-y}Mn_xCo_yO_2$ prepared by this study (SH-NMC). In addition, CP-NMC622 is an abbreviation for commercialized $LiNi_{0.6}Mn_{0.2}Co_{0.2}O_2$ produced by the general coprecipitation-heat treatment method. For consult, SH-NMC, SH-NMF and SH-NMA stand for $Li_{1-x}Ni_{1-x-y}Mn_xCo_yO_2$, $Li_{1-x}Ni_{1-x-y}Mn_xFe_yO_2$ and $Li_{1-x}Ni_{1-x-y}Mn_xAl_yO_2$ prepared by this study, respectively. According to Coulomb's law, as the positive and negative charges increase, the attraction between the positive and negative charges strengthens. Therefore, as the Ni oxidation number increases, the electron binding energy required to separate electrons from Ni ion increases. According to the results of the Ni XANES spectroscopy analysis in Figure 5, the Ni oxidation numbers of NiO, CP-NMC, and SH-NMC are +2, value between +2 and +3 (indicating the presence of both Ni^{2+} and Ni^{3+}), and +3, respectively.

Mn XANES spectroscopy results and Co XANES spectroscopy results of CPNMC and SH-NMC are summarized in Figs. 6 and 7, respectively. According to the results of Mn and Co XANES spectroscopy, the Mn and Co oxidation numbers of CPNMC are +4 and +3, respectively, as well as the Mn and Co oxidation numbers of SHNMC are also +4 and +3.

Moreover, the Ni, Mn, and Co XANES spectroscopy results of SH-NMC show that Ni^{3+}, Mn^{4+}, and Co^{3+} are all located in octahedral sites through their pre-edge absence and white line shapes, as well as there is no hybridization of *d* electron orbits and *p* electron orbits.

Consequently, it is confirmed that layered crystal structure $Li_{1-x}Ni_{1-x-y}Mn_xCo_yO_2$ ($0.1 \le x + y \le 0.5$) with Ni^{3+}, Mn^{4+}, and Co^{3+} may be prepared.

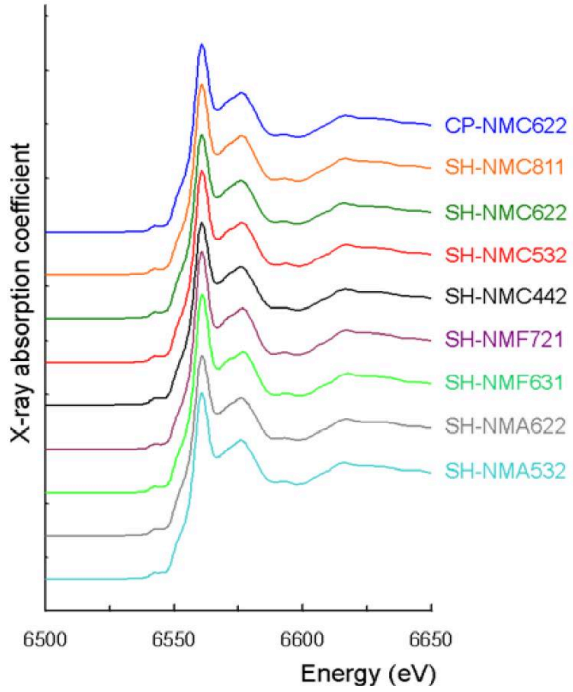

Figure 6: Mn XANES spectroscopic results of commercialized $LiNi_{1-x-y}Mn_xCo_yO_2$ (CP-NMC) manufactured by the general coprecipitation-heat treatment method and $Li_{1-x}Ni_{1-x-y}Mn_xCo_yO_2$ (SH-NMC) prepared by this study

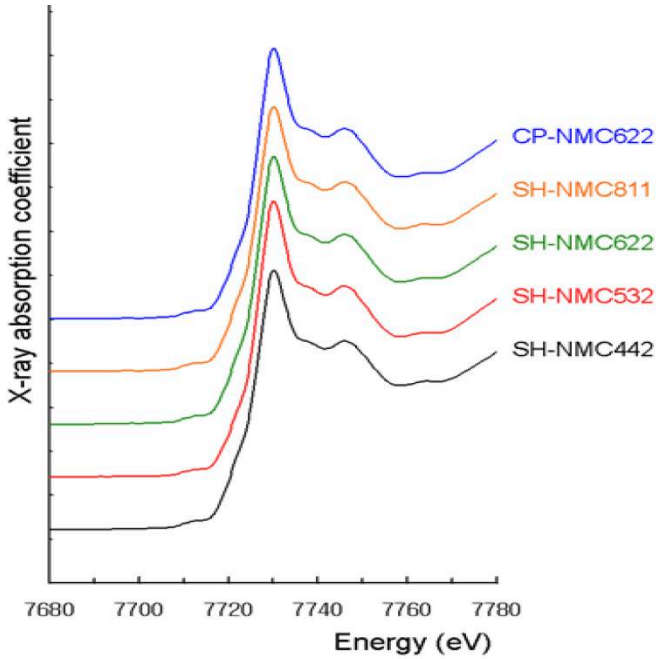

Figure 7: Co XANES spectroscopic results of commercialized $LiNi_{1-x-y}Mn_xCo_yO_2$ (CP-NMC) manufactured by the general coprecipitation-heat treatment method and $Li_{1-x}Ni_{1-x-y}Mn_xCo_yO_2$ (SH-NMC) prepared by this study

Figure 8 is the results of Fourier transform into r-space of k^3-weighted Ni K-edge extended X-ray absorption fine structure (EXAFS) spectroscopy information of NiO, CP-NMC, and SH-NMC. Figure 8 also represents the indirect support for Ni oxidation number of $Li_{1-x}Ni_{1-x-y}Mn_xCo_yO_2$ through the results of Ni-O bond length.

As the difference in oxidation number between cations and anions intensifies, the attraction between cations and anions becomes stronger, and the bond length between cations and anions becomes shorter. Thus, the fact that the Ni-O bond lengths of NiO, CP-NMC, and SH-NMC are gradually shortened in order means that the Ni oxidation num-

bers of NiO, CP-NMC, and SH-NMC are gradually increasing in order.

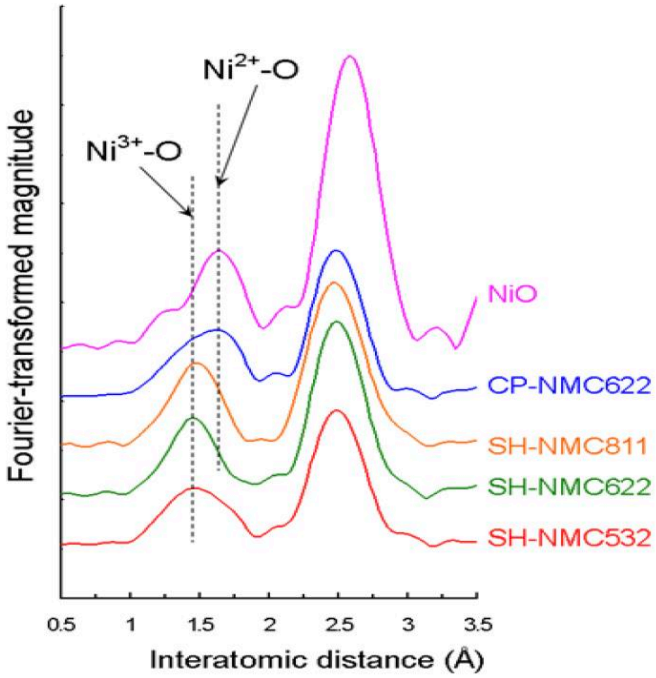

Figure 8: Results of Fourier transform into r-space of k^3-weighted Ni K-edge extended X-ray absorption fine structure (EXAFS) spectroscopy information of NiO, commercialized $LiNi_{1-x-y}Mn_xCo_yO_2$ (CP-NMC) manufactured by the general coprecipitation-heat treatment method, and $Li_{1-x}Ni_{1-x-y}Mn_xCo_yO_2$ (SH-NMC) prepared by this study

Ni, Mn, and Co have nuclear spin quantum numbers of 7/2, 5/2, and 3/2, respectively. Their nuclear proton spins have magnetic spin-spin interactions not only with neighboring proton spins but also with electron spins. Here, the difference between substances occurs. Ni^{3+} has six paired 3*d* electrons and one unpaired 3*d* electron, while Mn^{4+} has three unpaired 3*d* electrons. As Ni^{3+} and Mn^{4+} have unpaired electrons, both Ni^{3+} and Mn^{4+} exhibit paramagnetism. Therefore, magnetic spin-spin interaction can be performed. On the other hand, Co^{3+} and Ni^{2+} have diamagnetism because they have only six paired 3*d* electrons. The difference is shown in Figure 9 as single signal peak and multiple signal peaks, which are the Li magic angle spin nuclear magnetic resonance (Li MAS NMR) microstructure information.

As $Li_{1-x}Ni_{1-x-y}Mn_xCo_yO_2$ was prepared through a rapid hydroxide coprecipitation at the same solubility of nickel sulfate, manganese sulfate, and cobalt sulfate in 58^0C aqueous solution as well as a selective oxidation process of Ni^{2+} to Ni^{3+} without changing the states of Co^{3+} and Mn^{4+}, it is expected that $Li_{1-x}Ni_{1-x-y}Mn_xCo_yO_2$ was made of homogeneous arrangement of Ni^{3+}, Mn^{4+}, and Co^{3+}. By the way, $LiNi_{1-x-y}Mn_xCo_yO_2$ produced through general hydroxide coprecipitation at room temperature has a concentration gradient characteristic of each component due to the precipitation of each component in a different order depending on the difference in solubility of each component. Strictly, $LiNi_{1-x-y}Mn_xCo_yO_2$ with a concentration gradient is a mixture, not a solid solution capable of controlling material properties. For this reason, paramagnetic components and dimagnetic components are distinguished. In this case, the diamagnetic Co^{3+}, the diamagnetic Ni^{2+}, the paramagnetic Ni^{3+} and the paramagnetic Mn^{4+} are individually and locally concentrated, so the Li MAS NMR spectrum of $LiNi_{1-x-y}Mn_xCo_yO_2$ produced through general hydroxide coprecipitation at room temperature might show a combination of broad single signal peak and sharp multiple signal peaks. Because the Li MAS NMR spectrum of $Li_{1-x}Ni_{1-x-y}Mn_xCo_yO_2$ prepared by this study does not show such the combination, it is considered that $Li_{1-x}Ni_{1-x-y}Mn_xCo_yO_2$ prepared by this study was made of homogeneous arrangement of Ni^{3+}, Mn^{4+}, and Co^{3+}.

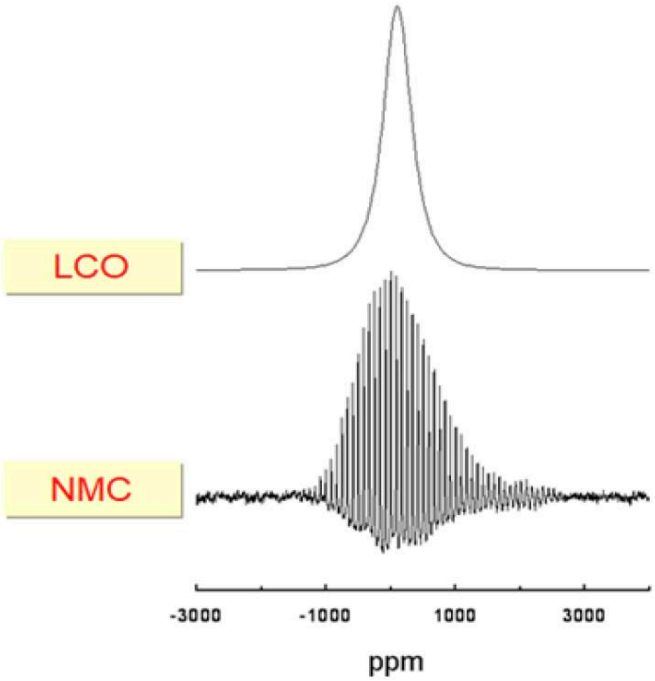

Figure 9: Li magic angle spin nuclear magnetic resonance (Li MAS NMR) spectra of $LiCoO_2$ and $Li_{1-x}Ni_{1-x-y}Mn_xCo_yO_2$

Figure 10 illustrates charge and discharge curves of a coin cell lithium secondary battery manufactured using SH-NMC811 as a cathode active material at 0.2C rate and 25^{0}C. The theoretical discharge capacity of a lithium secondary battery manufactured with $LiNi_{0.8}Mn_{0.1}Co_{0.1}O_2$ is 275.47 mAh/g, and the actual discharge capacity of a lithium secondary battery manufactured with SHNMC811 is 261.84 mAh/g. This is 95.1% of the theoretical discharge capacity per weight. Considering the partially irreversible energy conversion that always occurs in the first charging and discharging cycle, the coulombic efficiency ((discharge capacity)/(charge capacity)) and energy efficiency ([(coulombic efficiency)x(average discharge potential)]/(average charge potential)) of the lithium secondary battery manufactured using SH-NMC811, evaluated from second charging and discharging cycle to 40 charging and discharging cycles, are 99.7% and 99.2%, respectively, which represent very high energy conversion efficiency and also very high battery capacity retention rates. The partially irreversible conversion caused by the formation of solid electrolyte interphase (SEI) films is a necessary evil that inevitably contributes to the stabilization, safety and capacity decrease of a lithium secondary battery [1].

Figure 11 shows charge and discharge curves of a coin cell lithium secondary battery manufactured using SH-NMC622 as a cathode active material at 0.2C rate and 25^{0}C. The theoretical discharge capacity of a lithium secondary battery manufactured with $LiNi_{0.6}Mn_{0.2}Co_{0.2}O_2$ is 276.48 mAh/g, and the actual discharge capacity of a lithium secondary battery manufactured with SH-NMC811 is 242.73 mAh/g. This is 87.8% of the theoretical discharge capacity per weight. The lithium secondary battery produced with SH-NMC622 also experiences typical irreversible conversion in the first charging and discharging cycle. From the second charging and discharging cycle onwards, it demonstrates good stability, with high energy conversion efficiency and a nice battery capacity maintenance rate.

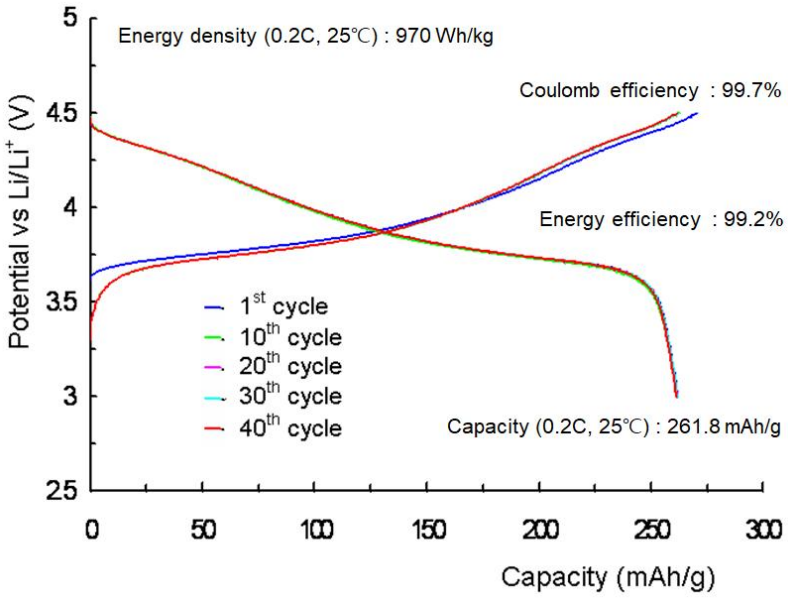

Figure 10: charge and discharge curves of a coin cell lithium secondary battery manufactured using SH-NMC811 as a cathode active material at 0.2C rate and 25^{0}C

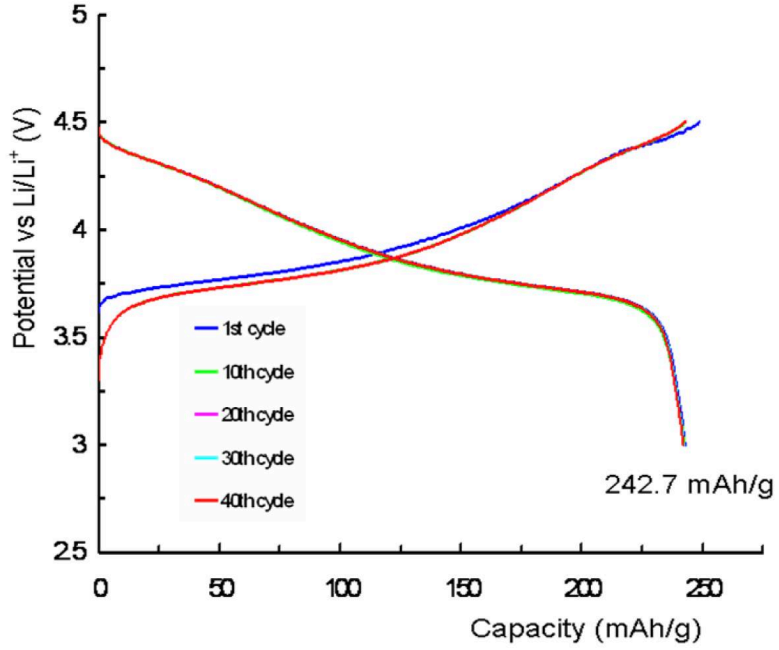

Figure 11: charge and discharge curves of a coin cell lithium secondary battery manufactured using SH-NMC622 as a cathode active material at 0.2C rate and 25^{0}C

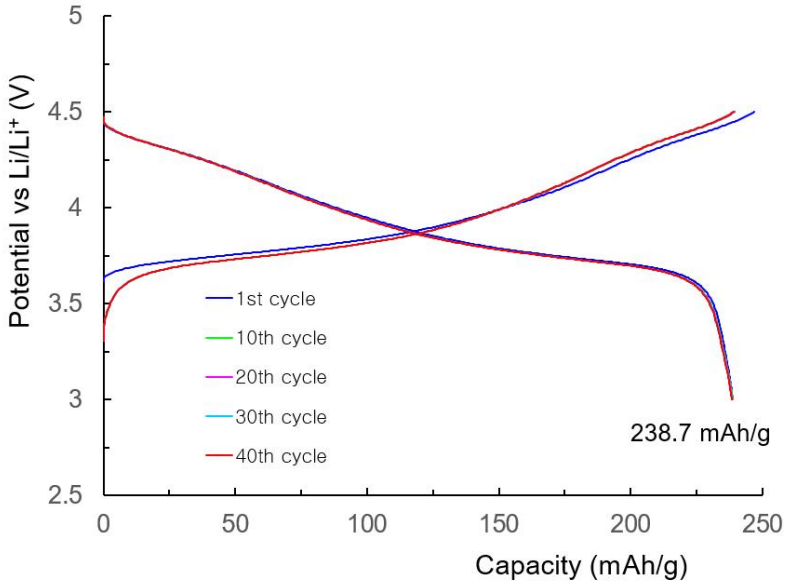

Figure 12: charge and discharge curves of a coin cell lithium secondary battery manufactured using SH-NMC523 as a cathode active material at 0.2C rate and 25^{0}C

Figure 12 illustrates charge and discharge curves of a coin cell lithium secondary battery manufactured using SH-NMC523 as a cathode active material at 0.2C rate and 25^{0}C. The theoretical discharge capacity of a lithium secondary battery manufactured with $LiNi_{0.5}Mn_{0.2}Co_{0.3}O_2$ is 276.42 mAh/g, and the actual discharge capacity of a lithium secondary battery manufactured with SH-NMC523 is 238.69 mAh/g. This is 86.3% of the theoretical discharge capacity per weight. The lithium secondary battery produced with SH-NMC523 also experiences typical irreversible conversion in the first charging and discharging cycle. From second charging and discharging cycle to 40 charging and discharging cycles, it demonstrates a remarkable stability, a superior energy conversion efficiency, and an amazing battery capacity maintenance rate of 99.8%.

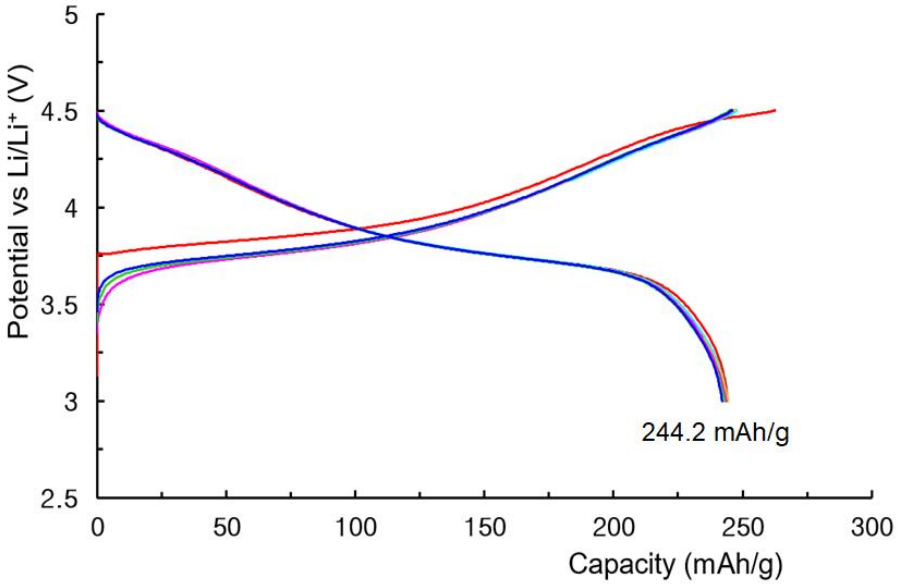

Figure 13: charge and discharge curves of a coin cell lithium secondary battery manufactured using SH-NMC523 as a cathode active material at 0.2C rate and 60^{0}C

Figure 13 shows charge and discharge curves of a coin cell lithium secondary battery manufactured using SH-NMC523 as a cathode active material at 0.2C rate and 60^0C. The theoretical discharge capacity of a lithium secondary battery manufactured with $LiNi_{0.5}Mn_{0.2}Co_{0.3}O_2$ is 276.42 mAh/g, and the actual 60^0C discharge capacity of a lithium secondary battery manufactured with SH-NMC523 is 244.22 mAh/g. This is 88.4% of the theoretical discharge capacity per weight. Unlike charging and discharging at 25^0C, the lithium secondary battery manufactured with SHNM-C523 exhibits very slight decrease battery capacity from the second charging and discharging cycle onwards at 60^0C.

Conclusion

An application of a lithium secondary battery manufactured with $LiNi_{1-x-y}Mn_xCo_yO_2$ is limited by intrinsic disadvantages of $LiNi_{1-x-y}Mn_xCo_yO_2$. To overcome the intrinsic disadvantages of $LiNi_{1-x-y}Mn_xCo_yO_2$ such as inappropriate but stable oxidation state of Ni^{2+} as well as uneven arrangement of Ni, Mn, and Co within $LiNi_{1-x-y}Mn_xCo_yO_2$, the solubility control according to coprecipitation temperature for homogeneous arrangement of Ni, Mn, and Co, as well as the selective oxidation control from Ni^{2+} to Ni^{3+} without changing the states of Co^{3+} and Mn^{4+} are established. In this way, single-phase layered crystal structure $Li_{1-x}Ni_{1-x-y}Mn_xCo_yO_2$ ($0.1 \le x + y \le 0.5$) with homogeneous arrangement of Ni^{3+}, Mn^{4+}, and Co^{3+} has been prepared and characterized by means of XRD, XANES, EXAFS, and Li MAS NMR.

The battery performance of the $Li_{1-x}Ni_{1-x-y}Mn_xCo_yO_2$ ($0.1 \le x + y \le 0.5$) obtained by the developed preparation method shows a maximum available capacity of 262mAh/g and a capacity retention rate of 99.7% in 40 charging and discharging cycles. Additionally, the battery capacity of the lithium secondary battery made with $Li_{1-\alpha}Ni_{1-x-y}Mn_xCo_yO_2$ increases as the ratio of Ni increases.

Acknowledgement

This work was supported by research fund of Chungnam National University.

References

1. Park JK, Doh CH, Han KS, Hong YS, Kang KS et al. (2012) Principles and applications of lithium secondary batteries, John Wiley & Sons.

2. Min K, Kim K, Jung C, Seo SW, Song YY et al. (2016) A Comparative Study of Structural Changes in Lithium Nickel Cobalt Manganese Oxide as a Function of Ni Content during Delithiation Process, J. Power Sources 315: 111-9.

3. Li W, Erickson EM, Manthiram A (2020) High-nickel Layered Oxide Cathodes for Lithium-based Automotive Batteries, Nature Energy 5: 26-34.

4. Sun YK, Myung ST, Kim MH, Prakash J, Amine K (2005) Synthesis and Characterization of Li[(Ni0.8Co0.1Mn0.1)0.8(Ni0.5Mn0.5)0.2]O2 with the Microscale Core-shell Structure as the Positive Electrode Material for Lithium Batteries, J. Electrochem. Soc 127: 13411-8.

5. Koyama Y, Yabuuchi N, Tanaka I, Adachi H, Ohzuku T (2004) Solid-State Chemisty and Electrochemistry of LiCo1/3Ni1/3Mn1/3O2 for Advanced Lithium-Ion Batteries I. First-Principles Calculation on the Crystal and Electronic Structures, J. Electrochem. Soc 151: 1545-51.

6. Ohzuku T, Ueda A, Nagayama M (1994) Electrochemistry and Structural Chemistry of LiNiO2 (R-3m) for 4V Secondary Lithium Cells, J. Electrochem. Soc 140: 1862-70.

7. Thackeray MM, Kang SH, Johnson CS, Vaughey JT, Benedek R, Hackney A (2007) Li2MnO3-stabilized LiMO2 (M = Mn, Ni, Co) Electrodes for Lithium-Ion Batteries, J. Mater. Chem 17: 3112-25.

8. Anansuksawat N, Chiochan P, Homlamai K, Joraleechanchai N, Tejangkura W, Sawangphruk M (2023) Reducing Intrinsic Drawbacks of Ni-rich Layered Oxide with a Multifunctional Materials Dry-coating Strategy, J. Power Sources 554: 232324.

9. Han E, Li Y, Zhu L, Zhao L (2014) The Effect of MgO Coating on Li1.17Mn0.48Ni0.23Co0.12O2 Cathode Material for Lithium Ion Batteries, Solid State Ionics 255: 113-9.

10. Chen Y, Zhang Y, Chen B, Wang Z, Lu C (2014) An Approach to Application for LiNi0.6Co0.2Mn0.2O2 Cathode Material at High Cutoff Voltage by TiO2 Coating, J. Power Sources 256: 20-7.

11. Hu SK, Cheng GH, Cheng MY, Hwang BJ, Santhanam R (2009) Cycle Life Improvement of ZrO2-coated Spherical LiNi1/3Co1/3Mn1/3O2 Cathode Material for Lithium Ion Batteries, J. Power Sources 188: 564-9.

12. Kim UH, Lee SB, Ryu JH, Yoon CS, Sun YK (2023) Optimization of Ni-rich Li[Ni0.92 xCo0.04Mn0.04Alx]O2 Cathodes for Lithium-ion Batteries, J. Power Sources 564: 232850.

13. Guilmard M, Rougier A, Grüne M, Croguennec L, Delmas C (2003) Effects of Aluminum on the Structural and Electrochemical Properties of LiNiO2, J. Power Sources 115: 305-14.

14. Vadivel S, Srimanon K, Sawangphruk M (2022) Comparison of the Structural and Electrochemical Properties of Layered Li[NixCoyMnz]O2 (x = 1/3, 0.5, 0.6, 0.7, 0.8 and 0.85), J. Power Sources 537: 231526.

15. Noh HJ, Youn SJ, Yoon CS, Sun YK (2013) Comparison of the Structural and Electrochemical Properties of Layered Li[NixCoyMnz]O2 (x = 1/3, 0.5, 0.6, 0.7, 0.8 and 0.85), J. Power Sources 233: 121-30.